AGU100 ADVANCING EARTH AND SPACE SCIENCE

Geophysical Research Letters

RESEARCH LETTER
10.1029/2018GL079324

Key Points:
- An idealized advection-diffusion model of a passive tracer can be used to study probability distributions of temperature
- A changing equator-to-pole temperature gradient impacts temperature variance only, and not higher order moments of the distribution
- The poleward motion of eddy stirring latitude causes a shift toward negative skewness throughout the midlatitudes

Supporting Information:
- Figure S1
- Figure S2
- Figure S3
- Supporting Information S1
- Supporting Information S2

Correspondence to:
M. Linz,
mlinz@atmos.ucla.edu

Citation:
Linz, M., Chen, G., & Hu, Z. (2018). Large-scale atmospheric control on non-Gaussian tails of midlatitude temperature distributions. *Geophysical Research Letters*, *45*. https://doi.org/10.1029/2018GL079324

Received 21 JUN 2018
Accepted 14 AUG 2018
Accepted article online 24 AUG 2018

Large-Scale Atmospheric Control on Non-Gaussian Tails of Midlatitude Temperature Distributions

Marianna Linz[1], **Gang Chen**[1], **and Zeyuan Hu**[2,3]

[1]Department of Atmospheric and Oceanic Sciences, University of California, Los Angeles, CA, USA, [2]Department of Atmospheric and Oceanic Sciences, Peking University, Beijing, China, [3]Department of Earth and Planetary Sciences, Harvard University, Cambridge, MA, USA

Abstract Observed surface temperature distributions are non-Gaussian, which has important implications for the likelihood of extreme events in a changing climate. We use a two-dimensional advection-diffusion model of temperature stirred by stochastically generated Rossby waves with a sustained background temperature gradient to explore non-Gaussian temperature distributions. We examine how these distributions change with changes to thermal relaxation and eddy stirring. Weakening the background temperature gradient leads to decreased variance but no changes in other moments, while the eddy properties affect both the variance and skewness. A poleward movement of eddy stirring latitude leads to reduced skewness for most latitudes, implying a shift toward longer negative tails in temperature distributions, all else being equal. In contrast, the dependence of temperature skewness on eddy speed is a nuanced, nonlinear relationship.

Plain Language Summary Global warming is expected to cause changes in extreme events. In this study, we use a simple model to explore how local extreme temperatures change with changes to large-scale wind and temperature patterns. Particularly, we are interested in the reasons that some regions have more extreme cold events than extreme warm events (and vice versa) and whether or not that asymmetry between hot and cold events will change. Although the model presented in this study is very simple, it qualitatively captures the statistics of present-day temperatures and may be regarded as a prototype for our understanding of how thermal and circulation changes impact extreme values. Our results show that the shifts in the circulation expected with global warming change both how often extreme temperatures occur and the asymmetry between hot and cold extremes. These results suggest caution in applying present-day temperature statistics to predicting future extremes.

1. Introduction

Climate change impacts not only the mean surface temperature but also its probability distribution with important implications for the frequency of cold air outbreaks in winter and heat waves in summer (Alexander & Perkins, 2013; Kretschmer et al., 2018; Rhines et al., 2017; Ruff & Neelin, 2012). With global warming, climate models predict reduced surface temperature variance in midlatitudes, which may be attributed to the decreased equator-to-pole temperature gradient from Arctic amplification (e.g., Schneider et al., 2015; Screen, 2014). Meanwhile, studies with idealized atmospheric models indicate that a poleward shift in jet latitude may cause an increase in cold temperature extremes (Garfinkel & Harnik, 2017; Hassanzadeh & Kuang, 2015). Arctic warming is expected to cause equatorward movement in midlatitude zonal jets (e.g., Barnes & Screen, 2015), but global warming could also cause a poleward jet shift through tropical upper tropospheric warming (e.g., Sun et al., 2013). Furthermore, changes to jet meandering may play an important role. Francis and Vavrus (2012) hypothesize that a decrease in eddy speed, due to slower zonal jet speeds from Arctic warming, causes more frequent meandering in the midlatitude jet and associated cold extremes in winter. While there is no robust observational evidence for a hemispheric increase in jet meandering, regional increases in wave amplitude may be found (e.g., Chen et al., 2015; Xue et al., 2017). The separate effects of wave amplitude and eddy speed are difficult to disentangle using realistic models or data, and so a simple model is needed to isolate the roles of different mechanisms in setting temperature distributions.

While synoptic variability of temperature is often considered to have a Gaussian distribution (e.g., Schneider et al., 2015), observed temperature distributions at the surface are non-Gaussian in the Northern Hemisphere when unfiltered (Proistosescu et al., 2016) and in the Southern Hemisphere even with filtering to synoptic timescales (Garfinkel & Harnik, 2017). Changes in these distributions over the instrumental record have not always been simple shifts in mean and variance (McKinnon et al., 2016). Non-Gaussianity leads to important changes to the likelihood of extreme events with shifts in mean temperature under global warming (Loikith & Neelin, 2015).

The non-Gaussian temperature distributions in observations and climate models may be understood by transport and mixing of a passive tracer. Kimura and Kraichnan (1993) showed that non-Gaussian temperature distributions are expected with temperature as a passive tracer provided a nonuniform temperature gradient. McLaughlin and Majda (1996) solved analytically for the moments of the distribution of a passive scalar with a shear flow, finding nonzero skewness with nonzero space average of the initial temperature profile. Simple passive tracers subjected to advection-diffusion processes with a sustained background gradient can produce distributions with Gaussian cores and approximately exponential tails (e.g., Hu & Pierrehumbert, 2001; Pierrehumbert, 2000). Recently, using an initial value approach, Garfinkel and Harnik (2017) emphasized the process of synoptic temperature advection and the importance of eddy covariance between anomalous temperature and velocity. In this study, we present a model for understanding non-Gaussian temperature distributions in the Earth-like parameter regime. We use stochastically forced Rossby waves to advect a temperature tracer, in contrast to less realistic white/red noise velocity anomalies.

We present an advection-diffusion model of temperature stirred by midlatitude eddies in section 2, which qualitatively represents the processes necessary to create nonzero skewness in temperature. We use this model in section 3 to demonstrate that advection across any temperature gradient, including a linear one, can cause non-Gaussianity, provided that the eddy covariance terms are included. Then we examine the sensitivities of temperature distributions with changes to the background temperature gradient and thermal properties and to eddy position and speed in section 4. Finally, in section 5, we discuss the implications of this study.

2. Advection-Diffusion Model of Temperature

To understand long-tail and short-tail temperature distributions (e.g., Loikith & Neelin, 2015), we solve the advection-diffusion equation on the sphere using the pseudo-spectral method for temperature θ, with Newtonian relaxation to a prescribed equilibrium temperature profile:

$$\frac{\partial \theta}{\partial t} = -\mathbf{v} \cdot \nabla \theta - \frac{\theta - \theta_{eq}}{\tau} - \kappa \nabla^8 \theta, \tag{1}$$

where κ is the hyper-diffusion coefficient that results in a 0.1 day damping timescale on the smallest resolved spherical harmonic and τ is the thermal relaxation timescale. The model is run at T42 resolution. For most simulations described in the paper, we specify the equilibrium temperature profile with sine-squared latitudinal dependence to create a warmer equator and cooler poles:

$$\theta_{eq}^{S} = \theta_0 - \Delta\theta \sin^2 \phi, \tag{2}$$

where ϕ is latitude, $\theta_0 = 300K$, and the equator-to-pole temperature gradient $\Delta\theta$ varies between simulations (see Table 1).

We have also conducted simulations with the equilibrium temperature varying linearly with latitude:

$$\theta_{eq}^{L} = \theta_0 - 2\Delta\theta|\phi|/\pi. \tag{3}$$

The factor of 2 ensures the same equator-to-pole temperature gradient as θ_{eq}^{S}.

To mimic midlatitude eddies in the atmosphere, the advecting velocity is specified as stochastically forced Rossby waves with prescribed zonal wavenumber and zonal advective speed with the largest amplitude in midlatitudes. More specifically, the advecting velocity $\mathbf{v}$ is determined by solving a linearized forced-dissipative vorticity equation on the sphere (Chen et al., 2007):

$$\frac{\partial \zeta}{\partial t} = \frac{\bar{u}_A}{a}\frac{\partial \zeta}{\partial \lambda} - v\beta + r_s\zeta + \mathcal{F}. \tag{4}$$

Table 1
Summary of Idealized Model Parameters Modified in This Study

Parameter	Interpretation	Base values	Range
$\Delta\theta$	Equator-to-pole temperature gradient	45 K	30–65 K
u_A	Zonal speed of eddy stirring	12 m/s	2–22 m/s
ϕ_0	Stirring latitude	40°	35–50°
τ	Temperature relaxation timescale	8 days	4–14 days
k	Wavenumber of forcing	6	4–9

Note. All runs use the sine-squared equilibrium temperature profile θ^S_{eq}, equation (2), except one integration of the base run using the linear equilibrium temperature profile θ^L_{eq}, equation (3). Results for the first four parameters are discussed in this paper, and results for changing wavenumber are in supporting information Figure S2.

$\zeta = \mathbf{k} \cdot \nabla \times \mathbf{v}$ is the vorticity, where $\mathbf{k}$ is the vertical unit vector. $\bar{u}_A$ is a prescribed advective speed, a is the radius of the Earth, λ is longitude, $\beta = 2\Omega \cos\phi/a$, where Ω is the Earth's rotation rate, and r_s is the frictional dissipation rate $r_s = 1/2$ days^{-1}. We force the vorticity equation with a midlatitude wave forcing, $\mathcal{F}$, which we specify as

$$\mathcal{F} = A \exp\left[-\left(\frac{|\phi| - \phi_0}{\Delta\phi}\right)\right] \mathrm{Re}\left[\tilde{W}(t) \exp(ik\lambda)\right]. \quad (5)$$

$\tilde{W}(t)$ is white noise with unit variance. We fix the stirring amplitude as A=8e−10 and the meridional width of eddy stirring as $\Delta\phi = 10°$. The stirring latitude ϕ_0 and zonal wavenumber k are varied (Table 1). Wind magnitudes from this white noise forcing are quite variable from one time step to the next. However, some memory is built into the damping, which is parameterized to be considerably (3×) stronger than in similar models that use red noise forcing (Barnes et al., 2010; Vallis et al., 2004)

The base run (perturbed runs in section 4) has $\Delta\theta = 45$ (30–65) K, $\tau = 8$ (4–14) days, $\phi_0 = 40$ (35–50)°, $u_A = 12$ (2–22) m/s, and wavenumber 6 (4–9, supporting information), with the sine-squared form of equilibrium temperature, θ^S_{eq}. The choices of parameters for the base run were based on qualitative agreement with the Southern Hemisphere summertime location of peak temperature variance, location of zero-crossing of skewness, maintaining a realistic equator-to-pole temperature gradient, and a trade-off between larger variance and smaller magnitude of skewness.

To summarize, this is a two-dimensional advection-diffusion model of temperature, whose gradient is maintained by Newtonian relaxation to a prescribed zonally symmetric equator-to-pole temperature gradient and stirred by stochastically forced midlatitude Rossby waves with a wavenumber k spatial pattern and zonal advective speed, $\bar{u}_A$.

3. Non-Gaussian Temperature Distributions

3.1. Base Run Versus Observations

We explore the model's representation of processes of temperature advection and diffusion and midlatitude temperature statistics as compared with reanalysis. We focus on the Southern Hemispher summer, when the influence of zonally asymmetric forcing (e.g., land-sea contrast or topography) is small. Figure 1 shows the Southern Hemisphere 850 hPa temperature and horizontal winds from the ERA-Interim reanalysis (Dee et al., 2011) on 10 December 2001 in the top panel and a snapshot of model output for temperature and velocity from the base run in the bottom panel. Horizontal winds are deviations from the zonal means. Some differences are noticeable: the idealized model necessarily does not capture deviations from the wave-6 pattern, and advection of warm air from the equator is more symmetric with advection of cold air from high latitudes. In spite of the simplicity of the model, one can qualitatively see similarities between the idealized model and ERA-Interim; namely, the idealized model has similar temperature gradients and patterns of advection of warm and cold air by eddies—consider the resemblance of the wind and temperature patterns in the upper left quadrant of both plots.

As the model qualitatively captures the processes of temperature advection and diffusion, we examine the second and third moments of the temperature distributions. The summer (December–January–February)

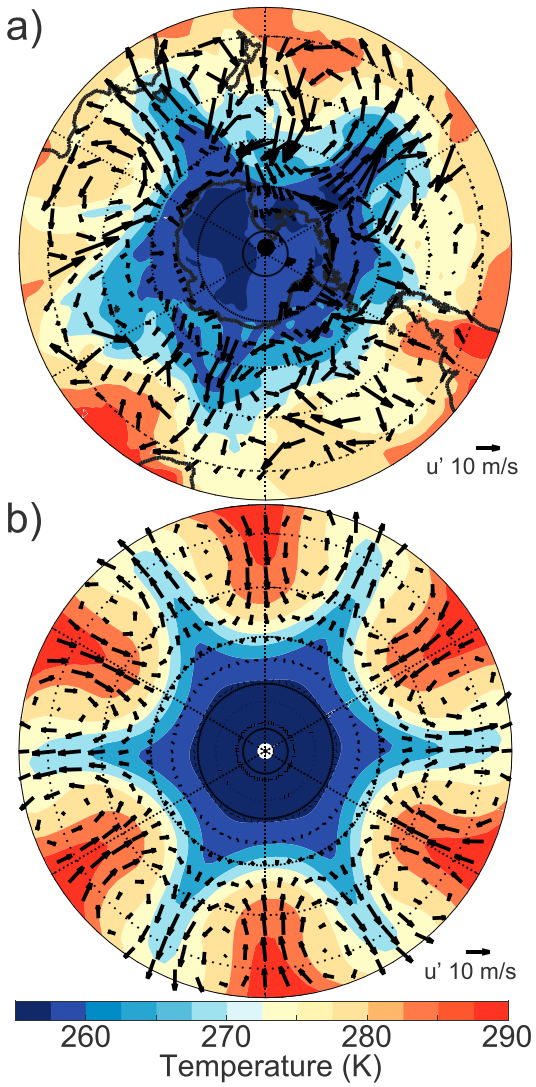

Figure 1. Temperature (in color) and horizontal winds (in arrows) from the Southern Hemisphere for (a) ERA-Interim at 850 hPa on 10 December 2001 and (b) a snapshot from the base run of the advection-diffusion model of temperature (see section 2). The temperature contour is every 2.5 K. Horizontal winds have the zonal mean velocity subtracted.

average patterns of Southern Hemisphere variance and skewness from ERA-Interim are shown in the left column of Figure 2. These are relatively zonally symmetric except over land, with a maximum in variance around 45°S. The temperature skewness is negative equatorward of the maximum variance and positive poleward of the maximum variance. In the right column of Figure 2, the zonal means of these moments are shown in the dashed black line. The blue line shows the zonal mean variance and skewness for the *base* run of the idealized model. The structure of the variance is different than in the reanalysis, with a broader peak partly due to a more gradual equilibrium temperature gradient in the idealized model. The skewness is negative equatorward of the maximum in variance and positive poleward, with the same latitude of zero-crossing as the reanalysis.

3.2. Causes of Non-Gaussian Distributions

Non-Gaussian temperature distributions can arise for many reasons. The first hypothesis we tested is the nonuniform temperature gradient (e.g., Kimura & Kraichnan, 1993). We, however, find that even a linear temperature gradient will lead to nonzero skewness in our system with localized advection. The results for variance and skewness from the linear background temperature gradient are shown in the red lines in the right column of Figure 2. Although the sine-squared background temperature leads to a larger variance than the linear temperature gradient due to a larger temperature gradient around 45°, the linear temperature gradient nevertheless yields almost the same skewness.

Second, because distributions of the large-scale circulation are observed to be non-Gaussian (e.g., Sura & Hannachi, 2015), an advection field with non-Gaussian statistics could be a simple explanation for non-Gaussian temperature distributions. The normalized and standardized probability distribution functions of meridional velocity and temperature anomalies at 850 hPa at 30° and 61.5°S are shown for summertime in ERA-Interim in the blue dashed line of Figures 3a and 3c and at 32° and 60°S for the idealized model in Figures 3b and 3d. For ERA-Interim, the distribution of meridional velocity is negatively skewed both poleward and equatorward of the jet, while the temperature distributions demonstrate both signs of skewness. For the idealized model, the wind statistics are Gaussian, but the temperature distributions are non-Gaussian with the same latitudinal variation of skewness as in ERA-Interim. Skewed temperature distributions arise with Gaussian distributions of advecting velocities.

Finally, we tested the Garfinkel and Harnik (2017) hypothesis that eddy terms are responsible for the nontrivial skewness that is positive equatorward and negative poleward of the jet. Similar to their initial value calculations in a temperature advection model, the nonlinear term in our advection-diffusion model is removed by replacing the temperature gradient in equation (1) with the zonal mean temperature gradient $\nabla\bar{\theta}$:

$$\frac{\partial\theta}{\partial t} = -\mathbf{v}\cdot\nabla\bar{\theta} - \frac{\theta-\theta_{eq}}{\tau} - \kappa\nabla^8\theta. \tag{6}$$

The resulting variance and skewness are shown in the purple dotted line in the right column of Figure 2. Note that although the variance is now greater, skewness is zero. The temperature gradient is much stronger, since advection no longer suppresses it, causing the increased variance. We conclude that non-Gaussian temperature distributions in the Southern Hemisphere summer likely arise from covariance between anomalous temperature and advecting velocity rather than nonuniform temperature gradient or non-Gaussian advecting velocities.

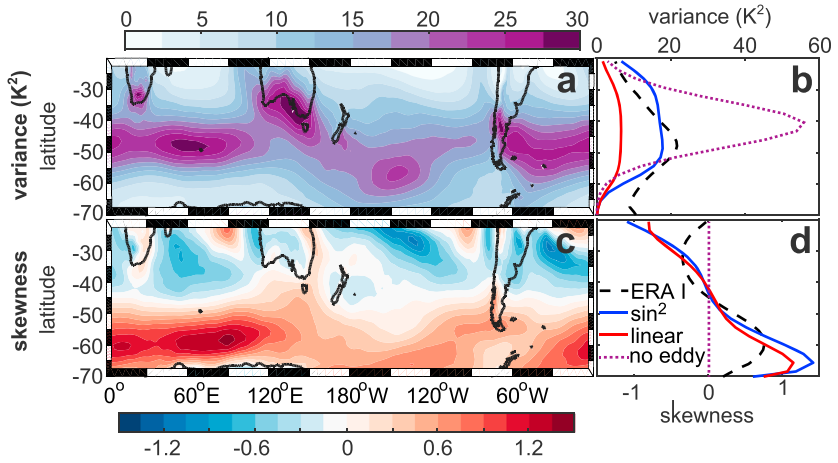

Figure 2. ERA-Interim December–January–February spatial patterns of (a) variance and (c) skewness of temperature at 850 hPa. Contours in (a) are every 2.5 K and in (c) are every 0.15. The zonal mean of these is shown in the dashed black line in (b) and (d), respectively. The colored lines show the zonal mean of variance and skewness of temperature for three simulations of the advection-diffusion model of temperature, all with the base run parameters: the blue solid line is the standard base run, the red solid line has a linear equilibrium temperature θ_{eq}^{L} given by equation (3), and the purple dashed line has advection of the mean temperature gradient only as specified in equation (6).

4. How Does the Distribution Change With Thermal Relaxation and Eddy Stirring?

We explore the dependence of variance and skewness of the temperature distributions on thermal relaxation (i.e., the equator-to-pole temperature gradient and thermal damping timescale) and eddy stirring (i.e., the location and the phase speed of vorticity anomalies). In reality, thermal perturbations are related to winds via the thermal wind relationship, but the two effects can be studied independently in our simple model.

4.1. Thermal Relaxation

The Newtonian relaxation to an equilibrium temperature is a gross approximation of radiation and convection. We explore the impact of the changing equator-to-pole temperature gradient independently of changes

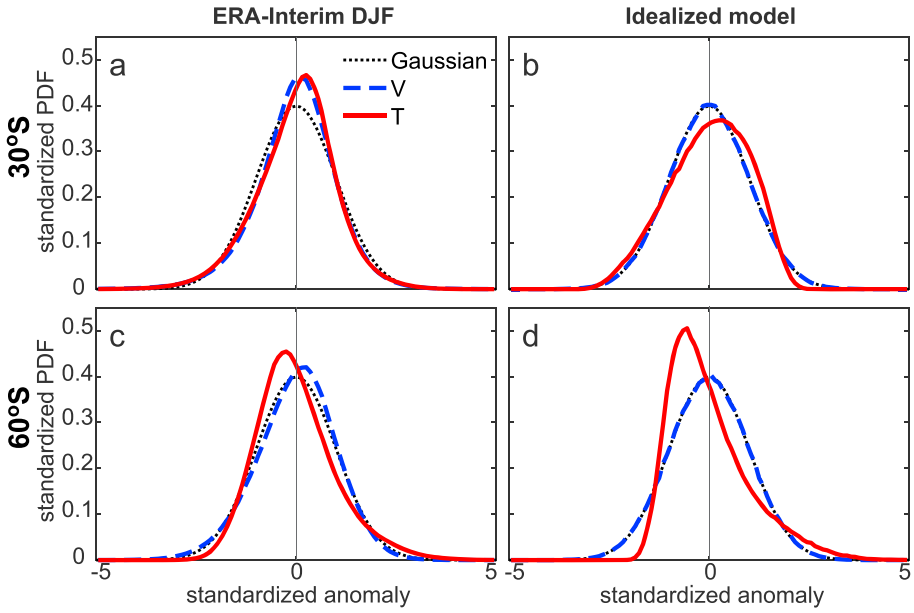

Figure 3. Zonally averaged PDFs for temperature (red solid line) and wind (blue dashed line) for ERA-Interim at 850 hPa at (a) 30° and (c) 61.5°S and for the idealized model base run at (b) 32°, and (d) 60°S. Distributions have been normalized by their standard deviations. The black dotted line shows the standard Gaussian distribution. PDF = probability density function; DJF = December–January–February.

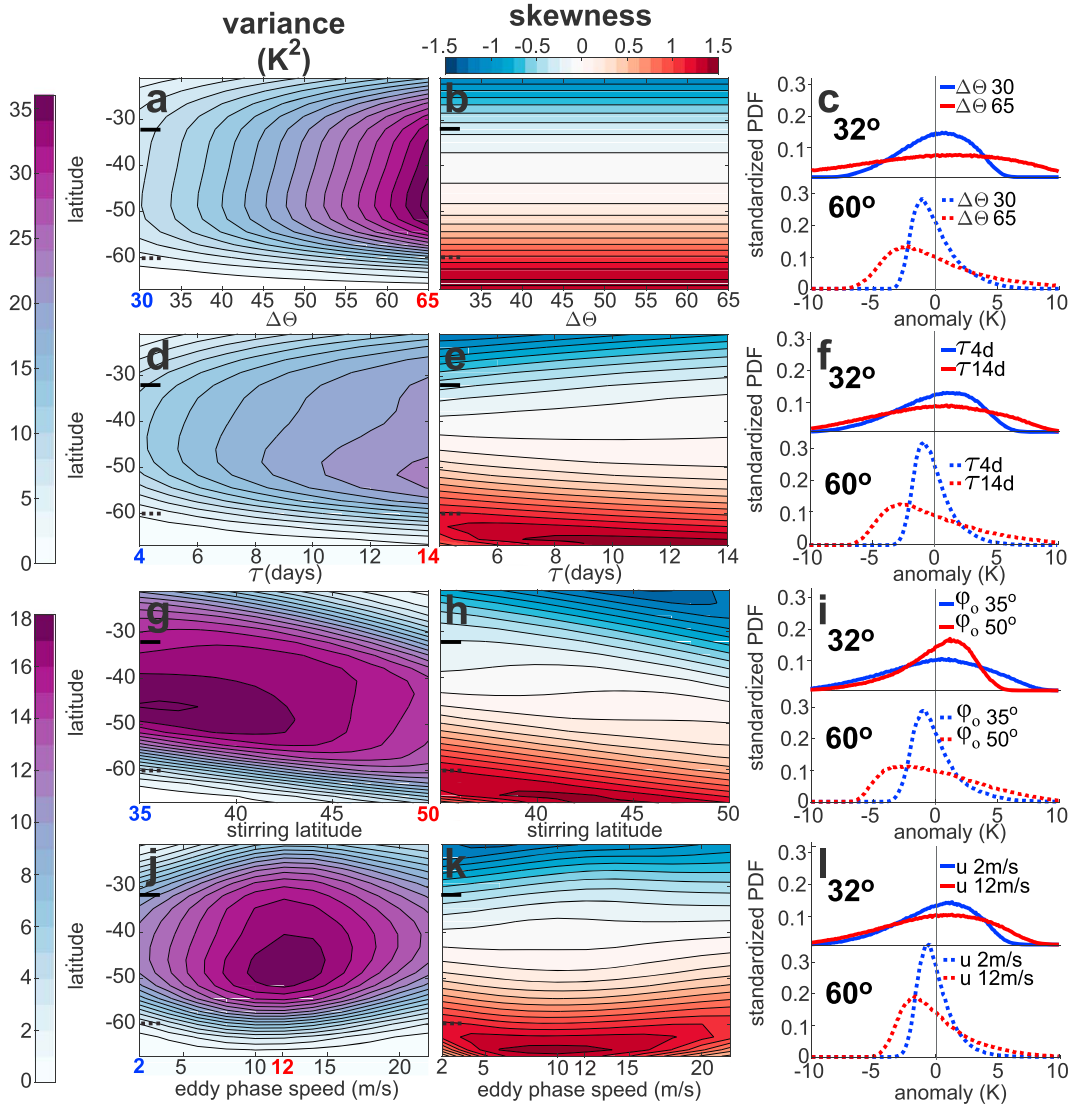

Figure 4. Zonal mean variance (first column) and skewness (second column) of temperature as a function of latitude for the idealized model with varying parameters. The third column shows the distributions of temperature anomalies at 32° (solid, upper panel) and 60° (dashed, lower panel) for different values of the parameter in each row as indicated by the legends and by colored numbers on the *x* axis. (a)–(c) show changes with varying equator-to-pole temperature gradient ($\Delta\theta$). (d)–(f) show changes with varying thermal relaxation. (g)–(i) show changes with stirring location. (j)–(l) show changes with varying eddy phase speed. Variance contours for (a) and (d) are every 2 K^2 and for (g) and (j) are 1 K^2. Skewness contours are every 0.15. See Figure S3 for distributions of standardized anomalies. PDF = probability density function.

to winds. The dependence of the variance and skewness on the changing equator-to-pole temperature gradient are shown in Figures 4a and 4b, respectively. An increase in the temperature gradient causes increased variance. In contrast, skewness is completely independent of this temperature gradient. The distributions of temperature anomalies at 32° and 60°S are shown in Figure 4c (top and bottom panels, respectively). Moving from a small equator-to-pole temperature gradient to a large one results in increased variance, but the higher order moments are unchanged. In reality, the changing gradient will necessarily change the flow, but changes to the asymmetry of temperature distributions and the likelihood of outliers (kurtosis) are a response to that change in flow.

Variations in the timescale of the Newtonian relaxation can conceptually be related to variations in local moisture and convection, heat capacity of the surface (whether land or ocean), and height of the boundary layer. Such differences generally will not be zonally symmetric. However, for the purposes of this study, we have

modified this thermal equilibrium timescale uniformly to get a first order understanding of its impacts, and these results are in Figures 4d–4f. With short timescales, perturbations are rapidly damped, causing the variance (Figure 4d) at low values of τ to be less than at higher values of τ. With the longest damping timescale, the variance is strongest poleward of the stirring latitude, and the midlatitude peak broadens in latitude, indicating larger increases in variance along the edges of the stirring. The increased damping timescale causes more symmetric distributions throughout the region close to the stirring (Figure 4e). Farther from the stirring, however, the increasing timescale leads to more dramatic asymmetry.

In summary, changes to the equilibrium temperature gradient and the temperature relaxation timescale mostly impact variance. The equilibrium temperature gradient only impacts the second moment, while changes to the relaxation timescale predominantly impact the second moment with a small impact on the third. For more significant changes to the third moment, changes to the flow field are necessary.

4.2. Eddy Stirring Location and Speed

The change in the second and third moments of the temperature distribution with location of the stirring is shown in Figures 4g and 4h. Away from its maximum, variance changes linearly with the stirring latitude; while near the maximum in temperature variance, the effect is different and related to the shape of the equilibrium temperature profile. Generally, at latitudes equatorward of the location of stirring, the variance decreases as this stirring moves poleward, while at latitudes poleward of the stirring location, the variance increases as the stirring moves poleward (Figure 4i). The skewness moves poleward with the stirring latitude, with small deviations from that behavior around 45°. Thus, at any given latitude equatorward of 65°, the skewness becomes more negative (or less positive) with a poleward shift in stirring latitude. This implies longer negative tails in midlatitude temperature distributions, consistent with the results from atmospheric dynamic core model studies (Garfinkel & Harnik, 2017; Hassanzadeh & Kuang, 2015).

The effects of eddy speed on the second and third moments of the temperature distribution are shown in Figures 4j and 4k, respectively. Temperature distributions equatorward and poleward of the stirring location are nearly identical with zonal advective speeds of 2 and 22 m/s, while at 12 m/s the distributions are quite different, marked especially by increased variance (comparison in Figure 4l). This nonlinear dependence of skewness on eddy speed indicates that the Francis and Vavrus (2012) hypothesis that a decrease in the eddy speed causes more extremes is not robust over a large range of changes to eddy speeds. This behavior can be explained in terms of the Rossby wave dispersion relation:

$$c = u_A - \frac{\beta}{k^2 + l^2}, \tag{7}$$

where c is the Rossby wave phase speed, u_A is the advecting velocity, k is the zonal wavenumber, and l is the meridional wavenumber. Assuming the maximum variance occurs when the waves are quasi-stationary (e.g., Wolf et al., 2018), that maximum will occur when $u_A \approx \beta/(k^2 + l^2)$. The meridional wavenumber is relatively consistent (between 3 and 4) for runs with the same zonal wavenumber; thus, a particular u_A maximizes variance.

5. Summary

We present a two-dimensional advection-diffusion model of temperature stirred by stochastically forced Rossby waves and relaxed to a zonally symmetric equilibrium temperature profile that can qualitatively recreate temperature transport and mixing and the first three statistical moments of observed temperature distributions. This model produces skewed temperature probability distributions despite the Gaussian velocity statistics, and with it we have demonstrated that such nonzero skewness arises from the eddy covariance, consistent with Garfinkel and Harnik (2017). This provides a physical basis to the non-Gaussian temperature tails found in observations in contrast to Schneider et al. (2015) who concluded synoptic near-surface temperature variations in midlatitudes are statistically indistinguishable from Gaussian.

We use this idealized model to separate the influences of changes to the thermal relaxation from the influences of changes to the advecting velocity itself. We found that changing the temperature gradient impacts the variance only. The thermal relaxation timescale impacts the variance as well, with small changes to skewness. In contrast, changes to the wind, and especially changes to the stirring location, affect the skewness more strongly. The impact of changes to the eddy speed on variance and skewness depends on the initial state.

This simple model may be regarded as a prototype for understanding how thermal and circulation changes impact temperature distributions and associated extreme values, especially for changes to eddy characteristics. Two of the most robust signals of climate change are the decreased equator-to-pole temperature gradient in the lower troposphere (e.g., Barnes & Screen, 2015) and the poleward motion of the jet associated with tropical upper tropospheric warming (e.g., Sun et al., 2013). In this model, the decrease in equator-to-pole temperature gradient alone has no impact on other moments, but it clearly decreases variance, corroborating predictions of future temperature variance by comprehensive climate models (e.g., Schneider et al., 2015; Screen, 2014). The poleward jet shift has a strong influence on the asymmetry of temperature distributions, and for most latitudes, results in a shift toward longer negative tails in temperature distributions, supporting results from atmospheric dynamical core studies (Garfinkel & Harnik, 2017; Hassanzadeh & Kuang, 2015). The hypothesis that a decrease in the eddy speed causes more extremes (Francis & Vavrus, 2012) is not robust over a large range of eddy speeds.

The barotropic model in this study is a simple tool for understanding passive tracer advection by midlatitude eddies. However, it does not include many features critical for regional temperature distributions, such as convection and adiabatic descent or the geography of the Northern Hemisphere, which has been linked to changes in temperature variance with Arctic amplification (e.g., Cohen et al., 2014; Horton et al., 2015; Screen et al., 2015). Future work with this model will include land-sea contrast and a simple treatment of vertical motion to enable comparisons with Northern Hemisphere data. Nevertheless, the results of this simple model that changes to both the variance and the skewness are inherent to global warming suggest caution in applying Gaussian statistics for predicting future extremes (e.g., Loikith & Neelin, 2015).

Acknowledgments
We are grateful to Cristi Proistosescu for helpful conversations. We thank two anonymous reviewers for their constructive comments. GC and ML are supported by NSF awards AGS-1742178 and AGS-1608775. Data are available at https://figshare.com/s/c51a3d1e5cee86610f49.

References

Alexander, L., & Perkins, S. (2013). Debate heating up over changes in climate variability. *Environmental Research Letters*, *8*(4), 041001.

Barnes, E. A., Hartmann, D. L., Frierson, D. M. W., & Kidston, J. (2010). Effect of latitude on the persistence of eddy-driven jets. *Geophysical Research Letters*, *37*, L11804. https://doi.org/10.1029/2010GL043199

Barnes, E. A., & Screen, J. A. (2015). The impact of Arctic warming on the midlatitude jet-stream: Can it? Has it? Will it? *Wiley Interdisciplinary Reviews: Climate Change*, *6*(3), 277–286. https://doi.org/10.1002/wcc.337

Chen, G., Held, I. M., & Robinson, W. A. (2007). Sensitivity of the latitude of the surface westerlies to surface friction. *Journal of the Atmospheric Sciences*, *64*(8), 2899–2915. https://doi.org/10.1175/JAS3995.1

Chen, G., Lu, J., Burrows, D. A., & Leung, L. R. (2015). Local finite-amplitude wave activity as an objective diagnostic of midlatitude extreme weather. *Geophysical Research Letters*, *42*, 10,952–10,960. https://doi.org/10.1002/2015GL066959

Cohen, J., Screen, J. A., Furtado, J. C., Barlow, M., Whittleston, D., Coumou, D., et al. (2014). Recent Arctic amplification and extreme mid-latitude weather. *Nature Geoscience*, *7*, 627–637.

Dee, D. P., Uppala, S. M., Simmons, A. J., Berrisford, P., Poli, P., Kobayashi, S., et al. (2011). The ERA-Interim reanalysis: Configuration and performance of the data assimilation system. *Quarterly Journal of the Royal Meteorological Society*, *137*(656), 553–597. https://doi.org/10.1002/qj.828

Francis, J. A., & Vavrus, S. J. (2012). Evidence linking Arctic amplification to extreme weather in mid-latitudes. *Geophysical Research Letters*, *39*, L06801. https://doi.org/10.1029/2012GL051000

Garfinkel, C. I., & Harnik, N. (2017). The non-Gaussianity and spatial asymmetry of temperature extremes relative to the storm track: The role of horizontal advection. *Journal of Climate*, *30*(2), 445–464. https://doi.org/10.1175/JCLI-D-15-0806.1

Hassanzadeh, P., & Kuang, Z. (2015). Blocking variability: Arctic amplification versus Arctic oscillation. *Geophysical Research Letters*, *42*, 8586–8595. https://doi.org/10.1002/2015GL065923

Horton, D. E., Johnson, N. C., Sing, D., Swain, D. L., Rajaratnam, B., & Diffenbaugh, N. S. (2015). Contribution of changes in atmospheric circulation patterns to extreme temperature trends. *Nature*, *522*, 465–469.

Hu, Y., & Pierrehumbert, R. T. (2001). The advection–diffusion problem for stratospheric flow. Part I: Concentration probability distribution function. *Journal of the Atmospheric Sciences*, *58*(12), 1493–1510. https://doi.org/10.1175/1520-0469(2001)058<1493:TADPFS>2.0.CO;2

Kimura, Y., & Kraichnan, R. H. (1993). Statistics of an advected passive scalar. *Physics of Fluids A: Fluid Dynamics*, *5*(9), 2264–2277. https://doi.org/10.1063/1.858530

Kretschmer, M., Coumou, D., Agel, L., Barlow, M., Tziperman, E., & Cohen, J. (2018). More-persistent weak stratospheric polar vortex states linked to cold extremes. *Bulletin of the American Meteorological Society*, *99*(1), 49–60. https://doi.org/10.1175/BAMS-D-16-0259.1

Loikith, P. C., & Neelin, J. D. (2015). Short-tailed temperature distributions over North America and implications for future changes in extremes. *Geophysical Research Letters*, *42*, 8577–8585. https://doi.org/10.1002/2015GL065602

McKinnon, K. A., Rhines, A., Tingley, M. P., & Huybers, P. (2016). The changing shape of Northern Hemisphere summer temperature distributions. *Journal of Geophysical Research: Atmospheres*, *121*, 8849–8868. https://doi.org/10.1002/2016JD025292

McLaughlin, R. M., & Majda, A. J. (1996). An explicit example with non-Gaussian probability distribution for nontrivial scalar mean and fluctuation. *Physics of Fluids*, *8*(2), 536–547. https://doi.org/10.1063/1.868806

Pierrehumbert, R. T. (2000). Lattice models of advection-diffusion. *Chaos: An Interdisciplinary Journal of Nonlinear Science*, *10*(1), 61–74. https://doi.org/10.1063/1.166476

Proistosescu, C., Rhines, A., & Huybers, P. (2016). Identification and interpretation of nonnormality in atmospheric time series. *Geophysical Research Letters*, *43*, 5425–5434. https://doi.org/10.1002/2016GL068880

Rhines, A., McKinnon, K. A., Tingley, M. P., & Huybers, P. (2017). Seasonally resolved distributional trends of North American temperatures show contraction of winter variability. *Journal of Climate*, *30*(3), 1139–1157. https://doi.org/10.1175/JCLI-D-16-0363.1

Ruff, T. W., & Neelin, J. D. (2012). Long tails in regional surface temperature probability distributions with implications for extremes under global warming. *Geophysical Research Letters*, *39*, L04704. https://doi.org/10.1029/2011GL050610

Schneider, T., Bischoff, T., & Płotka, H. (2015). Physics of changes in synoptic midlatitude temperature variability. *Journal of Climate*, *28*(6), 2312–2331. https://doi.org/10.1175/JCLI-D-14-00632.1

Screen, J. A. (2014). Arctic amplification decreases temperature variance in northern mid- to high-latitudes. *Nature Climate Change*, *4*(7), 577–582. https://doi.org/10.1038/nclimate2268

Screen, J. A., Deser, C., & Sun, L. (2015). Reduced risk of North American cold extremes due to continued Arctic sea ice loss. *Bulletin of the American Meteorological Society*, *96*, 1489–1503. https://doi.org/10.1175/BAMS-D-14-00185.1

Sun, L., Chen, G., & Lu, J. (2013). Sensitivities and mechanisms of the zonal mean atmospheric circulation response to tropical warming. *Journal of the Atmospheric Sciences*, *70*(8), 2487–2504. https://doi.org/10.1175/JAS-D-12-0298.1

Sura, P., & Hannachi, A. (2015). Perspectives of non-Gaussianity in atmospheric synoptic and low-frequency variability. *Journal of Climate*, *28*(13), 5091–5114. https://doi.org/10.1175/JCLI-D-14-00572.1

Vallis, G. K., Gerber, E. P., Kushner, P. J., & Cash, B. A. (2004). A mechanism and simple dynamical model of the North Atlantic Oscillation and annular modes. *Journal of Atmospheric Science*, *61*, 264–280.

Wolf, G., Brayshaw, D. J., Klingaman, N. P., & Czaja, A. (2018). Quasi-stationary waves and their impact on European weather and extreme events. *Quarterly Journal of the Royal Meteorological Society*. https://doi.org/10.1002/qj.3310

Xue, D., Lu, J., Sun, L., Chen, G., & Zhang, Y. (2017). Local increase of anticyclonic wave activity over northern Eurasia under amplified Arctic warming. *Geophysical Research Letters*, *44*, 3299–3308. https://doi.org/10.1002/2017GL072649